J Solid State Electrochem (2010) 14:1269–1277
DOI 10.1007/s10008-009-0930-2

ORIGINAL PAPER

Oxygen reduction on carbon nanomaterial-modified glassy carbon electrodes in alkaline solution

Ivar Kruusenberg · Jaan Leis · Mati Arulepp · Kaido Tammeveski

Received: 27 April 2009 / Revised: 7 July 2009 / Accepted: 25 August 2009 / Published online: 16 September 2009

Abstract Electroreduction of oxygen in alkaline solution on glassy carbon (GC) electrodes modified with different carbon nanomaterials has been studied. Electrochemical experiments were carried out in 0.1 M KOH employing the rotating disk electrode and rotating ring-disk electrode methods. The GC disk electrodes were modified with carbon nanomaterials using polytetrafluoroethylene as a binder. Four different carbon nanomaterials were used: multiwalled carbon nanotubes, carbon black powder, and two carbide-derived carbons (CDC). For the first time, the electrocatalytic behavior of CDC materials toward oxygen reduction is explored. Electrochemical characterization of the materials showed that all the carbon nanomaterial-modified GC electrodes are highly active for the reduction of oxygen in alkaline solutions.

Keywords Oxygen reduction · Electrocatalysis · Carbon nanomaterial · Carbide-derived carbon · Carbon nanotube

Introduction

Oxygen reduction has attracted much attention in electrochemistry due to its importance in electrochemical devices like fuel cells, metal-air batteries, and biosensors, in the electrosynthesis of hydrogen peroxide, and in other industrial processes [1–4]. Depending on the electrode material and the solution composition, the oxygen reduction reaction proceeds by a two-electron pathway or via "direct" four-electron pathway [5, 6]. The production of water by a four-electron oxygen reduction is used in fuel cells, while hydrogen peroxide is electrochemically generated by a two-electron reduction of oxygen. The mechanism of O_2 reduction is influenced by the electrode material and its surface properties as well as by the solution pH [1]. Caused by catalytically active properties of carbon materials for O_2 reduction at higher pHs, most of the oxygen reduction studies on carbon electrodes have been carried out in alkaline solution [7–19]. The electrochemical reduction of oxygen on carbon-based electrodes has received a long-standing interest and has been extensively studied. In alkaline solution, different types of carbon have wide research interest, such as glassy carbon, pyrolytic graphite, highly oriented pyrolytic graphite, boron-doped diamond, reticulated vitreous carbon, and other carbon materials as reviewed by Tryk et al. [20]. There have been recent efforts to characterize different carbon nanomaterials as possible electrocatalyst supports [21]. A number of activated carbons, carbon nanotubes, and other types of carbon along with a large variety of precursors and synthesis conditions rendered long and extensive systematic studies [22]. Carbon materials used for these studies range from conventional carbon powders, such as Vulcan XC72, Black Pearls BP2000, and Shawinigan carbon black and activated carbons, to fewer known carbon fibers and hard carbon spherules. With the scientific breakthrough of synthesis of nanostructured carbon materials, several new forms of carbons have been synthesized like carbon nanocapsules and carbon nanotubes [23, 24]. Carbon nanotubes (CNTs) have attracted a great deal of attention since their discovery

I. Kruusenberg · J. Leis · K. Tammeveski (✉)
Institute of Chemistry, University of Tartu,
Jakobi 2,
51014 Tartu, Estonia
e-mail: kaido@chem.ut.ee

J. Leis · M. Arulepp
Carbon Nanotech Ltd,
Riia 185,
51014 Tartu, Estonia

by Iijima [24] in 1991 as a new type of electrocatalytic material. Numerous studies have been made to investigate the electrochemical properties of CNTs, including the electrocatalysis of oxygen reduction [25–28]. The electrocatalytic properties of CNTs toward O_2 reduction are of great fundamental and practical importance, because of the possibility of using them as support material for various catalysts in fuel cell applications. As most of carbon materials, CNT-modified electrodes are active electrocatalysts for O_2 reduction in alkaline solution [29–31].

Recently, we have studied the electro chemical reduction of oxygen on multiwalled carbon nanotube (MWCNT)-modified electrodes in acid [25] and alkaline [29] solutions. The pH dependence of O_2 reduction on MWCNT-surfactant-modified glassy carbon electrodes has also been investigated [32]. The purpose of the present work is to study the reduction of O_2 on various carbon nanomaterials in alkaline solution. This is the first report on the electrocatalytic properties of carbide-derived carbon (CDC) materials for oxygen reduction.

Materials and methods

Synthesis and characterization of carbide-derived carbon

Aluminum carbide (Accumet, 325 mesh or Cerac, 1–5 μm of average particle size), with or without graphitization catalyst [33], was loaded in the horizontal quartz tube and was reacted with a flow of chlorine gas (99.999%) at a fixed temperature, which is indicated in Table 1. The by-product, $AlCl_3$, was evacuated by the flow of the excess chlorine. During the heating and cooling, the reactor was flushed with a slow stream of argon. After chlorination, the product was additionally treated with hydrogen at 800 °C to deeply dechlorinate the sample. Complete conversion of carbide into carbon was confirmed by the X-ray powder diffraction (XRD) measurements using CuKα radiation (λ= 1.54 Å). For convenience, these CDC materials are designated as C824 and C1551. The former material can be classified as "turbostratic" carbon, whereas the latter one forms nanobarrel-like structures.

The low-temperature N_2 sorption experiments were performed at −196 °C. The specific surface area (S_A) was calculated according to the Brunauer–Emmett–Teller theory up to the nitrogen relative pressure (P/P_0) of 0.2. The total volume of pores (V_p) was calculated at relative pressure (P/P_0) of 0.95 and the volume of micropores (V_μ) from t plot, using Harkins–Jura thickness values between 5 and 90 Å.

Transmission electron microscopy (TEM) studies were made with a JEOL JEM 3010 instrument operated at 300 kV. For the TEM measurements, small sample amounts were crushed in n-butanol, and a drop of the dispersion obtained was transferred to a perforated carbon film supported by a copper grid.

Electrode preparation

Rotating disk electrode (RDE) and the rotating ring-disk electrode (RRDE) techniques were used. For the RDE experiments, a glassy carbon (GC) disk of geometric area (A) of 0.2 cm^2 was employed. An interchangeable E6 series RRDE tip of GC disk–Pt ring (Pine Research Instrumentation, Inc., Grove City, PA, USA) was used for the RRDE measurements. A collection efficiency (N) of 0.25 was determined from measurements of hexacyanoferrate(III) reduction. Both the GC disk and Pt ring electrodes were polished to a mirror finish with 1.0, 0.3, and 0.05 μm alumina slurries (Buehler) followed by sonication in water for 5 min before use. Milli-Q water (Millipore, Inc.) was used throughout.

Four different carbon nanomaterials were used in the present study: multiwalled carbon nanotubes (MWCNTs), carbon black powder (Vulcan XC72R), and the CDC materials C824 and C1551. The S_A value of Vulcan XC72R (Cabot Corp.) was 254 $m^2 g^{-1}$. MWCNTs, purity >95%, diameter 30±10 nm, and length 5–20 μm, was a product of Nanolab, Inc. (Brighton, MA, USA). The nanotubes were treated by refluxing in a mixture of concentrated sulphuric and nitric acids (1:1, v/v) for 2 h at 55 °C and then for 3 h at 80 °C. Afterwards, the nanotubes were washed with Milli-Q water by centrifugation (3,000 rpm, 10 min) repeating it for several times. Finally, the MWCNTs were dried under vacuum for 15 h.

The GC disk electrodes were modified with carbon nanomaterials using aqueous suspensions of 4 mg cm^{-3} in the presence of 0.3% nonionic surfactant Triton X-100 (Sigma-Aldrich) and 0.4 mg cm^{-3} polytetrafluoroethylene (PTFE; Sigma-Aldrich). The surfactant was used to make a

Table 1 The physical parameters of Al_4C_3-derived carbons

Notation of CDC material	Origin of Al_4C_3	Catalyst $NiCl_2/CoCl_2/FeCl_3$ (mg g^{-1} (carbide))	T_{Cl} (°C)	S_A ($m^2 g^{-1}$)	V_p ($cm^3 g^{-1}$)	V_μ ($cm^3 g^{-1}$)
C824	Accumet	70/70/70	1,100	177	0.12	~0
C1551	Cerac	3.5/3.5/–	700	684	0.88	~0

uniform dispersion of nanocarbons. All the suspensions were sonicated for 1 h. Carbon nanomaterials were physically attached to the surface of electrodes by pipetting 10 μl aliquot of the suspension onto GC surface and allowing the solvent to evaporate in air. For the RDE measurements, the carbon nanomaterial-modified GC electrodes were heated at 80°C in an oven for 1 h before use. For the RRDE measurements, the modified GC electrodes were heated at 350°C for 0.5 h. At this temperature, the surfactant used decomposes [34].

Electrochemical measurements

A Pine Research Instrumentation AFMSRX rotator and MSRX speed controller were employed for the RDE and RRDE measurements. Experiments were controlled with the General Purpose Electrochemical System software, and the potential was applied with an Autolab potentiostat/galvanostat PGSTAT10 (Eco Chemie B.V., The Netherlands). A Pt foil served as the counter electrode, and reference electrode was a saturated calomel electrode. All potentials are referred to this electrode.

All the experiments were carried out in 0.1 M KOH (Aristar, BDH). The electrodes were electrochemically characterized by cyclic voltammetry in the electrolyte saturated with Ar (99.999%, AGA). Oxygen reduction was studied in the same solution saturated with O_2 (99.95%, AGA). For the RRDE measurements, the Pt ring electrode was activated before recording each scan by applying three potential cycles between −1.0 and 0.7 V at 0.1 Vs^{-1} in order to improve reliability in the determination of peroxide. The potential of the Pt ring electrode was kept under potentiostatic control at 0.55 V for peroxide detection.

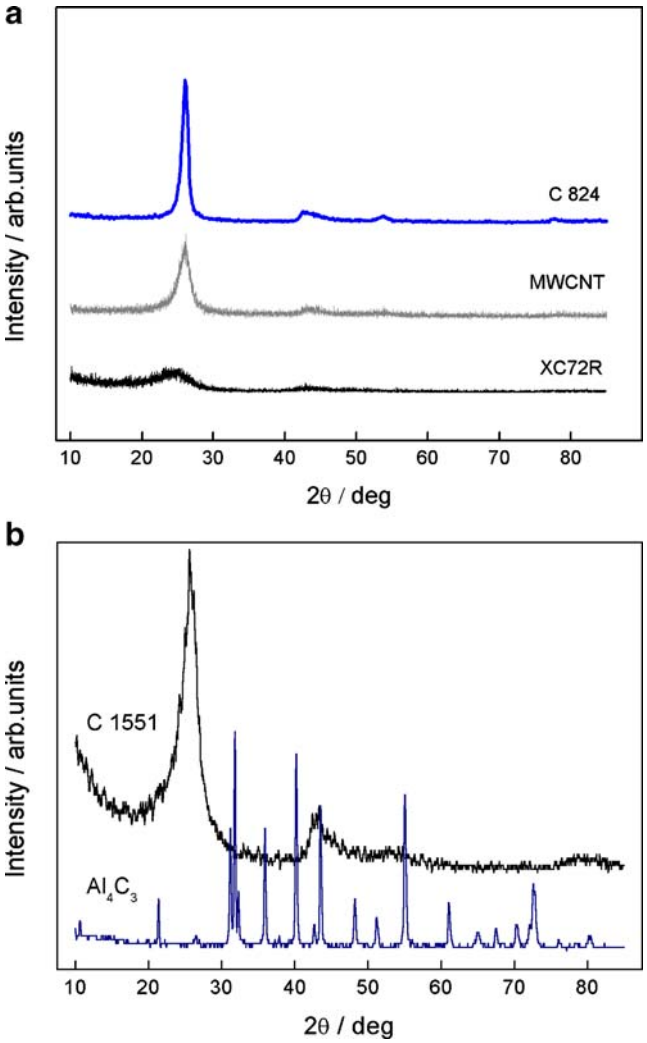

Fig. 1 Characteristic XRD patterns for carbon materials. **a** C824, MWCNT, and Vulcan XC72R. **b** C1551 and the precursor material, Al_4C_3

Results and discussion

XRD characterization of carbon nanomaterials

The example of XRD patterns of nanocarbons and the respective precursor material, Al_4C_3, are shown in Fig. 1. Figure 1a shows a typical powder XRD profile of the partially graphitic carbide-derived carbon (C824) and that of MWCNT and carbon black samples. As expected, the XRD peaks of commercial carbon powder (Vulcan XC72R) are rather broad and small, indicating that the material contains mostly amorphous carbon. There are some graphitic regions in this material which gives reflections at 24.5 and 43.5°. The nanotube material shows a somewhat higher peak of the 002 orientation. For both CDC materials, the 002 Bragg diffraction peak at 2Θ ~26° corresponds to parallel graphene layers although there is no graphite-like regularity. The 10 diffraction peak at 2Θ ~43° characterizes the 2D in-plane symmetry along the graphene layers. The graphitization for C1551 is much lower than for C824, therefore high ordered 004 and 11 graphite interlayer diffraction peaks are very weak. Also, the peak at 26° is much narrower for C824 (Fig. 1a). The formation of Al_4C_3-derived carbons proceeds by net reaction 1:

$$Al_4C_3 + 6Cl_2 = 3C + 4AlCl_3 \uparrow \quad (1)$$

Surface morphology of CDC samples

The surface morphology was examined by transmission electron microscopy (TEM) method. Figure 2 shows TEM micrographs of C1551 and MWCNT samples. One can see on the TEM image a large number of nanobarrels and small

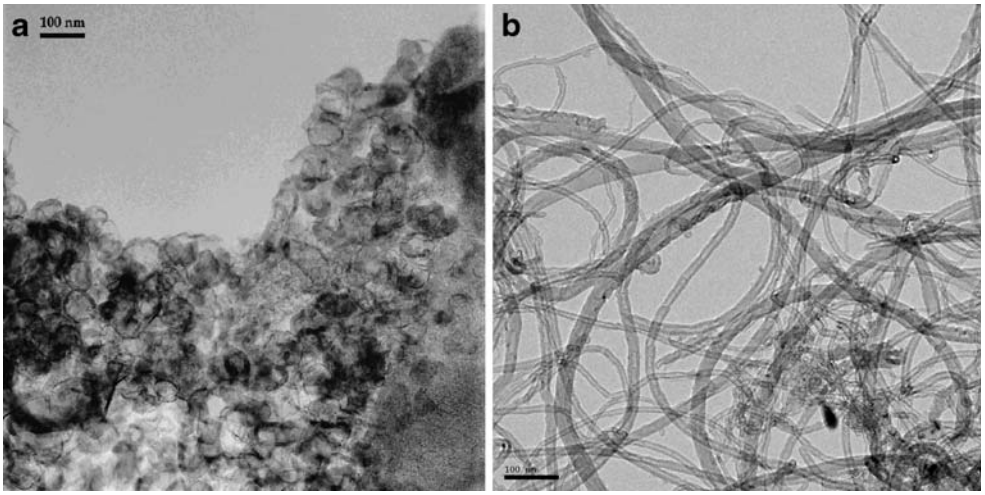

Fig. 2 TEM images of **a** C1551 and **b** MWCNT materials deposited on an amorphous carbon film

flake-looking particles of a CDC material (Fig. 2a). The TEM image revealed that this sample consisted of nanobarrels having sizes from 50 to 100 nm. However, there were also many particles that at a first view seemed to be amorphous, but at closer look were found to consist of small flakes which are actually nanobarrels sized about 10 nm. The thickness of the turbostratic carbon flakes varied from two to 15 graphene layers. The rest is mainly an intermediate between amorphous carbon and nanoparticles. Therefore, one may find several similarities between the XRD patterns from the nanocarbon-containing samples used in this study and those reported for MWCNTs. A typical TEM image of the acid-treated MWCNTs used in this work is also presented (Fig. 2b). The TEM micrograph indicates that the nanotube material is free of catalyst impurities.

Rotating disk electrode studies of O_2 reduction

The kinetics of the oxygen reduction reaction at carbon nanomaterial-modified electrodes was investigated using the RDE method. Figure 3 presents the RDE polarization curves for oxygen reduction on different carbon material-PTFE (MWCNT-PTFE, carbon black-PTFE, C824-PTFE, and C1551-PTFE)-modified GC electrodes in O_2-saturated 0.1 M KOH. These electrodes were heated at 80 °C for 1 h before electrochemical testing. The RDE results were rather similar for all the modified electrodes studied. The limiting current increases when the rotation rate increases, and there is a clear prewave present at low overpotentials. The second reduction wave on these materials starts at approximately −0.7 V.

For carbon nanomaterials C824 and C1551, a high reduction current was observed probably because of the high degree of graphitization, which leads to a mesoporous structure of these carbons. Mesoporous materials potentially lead to faster charge transfer rate as observed previously [35, 36], while the high surface area materials with a nonporous structure and fully accessible surface such as carbon onions were previously shown to have high response rates.

The number of electrons transferred per O_2 molecule (n) was calculated from the Koutecky–Levich (K–L) equation [37]

$$\frac{1}{I} = \frac{1}{I_k} + \frac{1}{I_d} = -\frac{1}{nFAkc^b_{O_2}} - \frac{1}{0.62nFAD^{2/3}_{O_2}\nu^{-1/6}c^b_{O_2}\omega^{1/2}} \quad (2)$$

where I is the measured current, I_k and I_d are the kinetic and diffusion-limited currents, respectively, k is the electrochemical rate constant for O_2 reduction, D_{O_2} is the diffusion coefficient of oxygen (1.9×10^{-5} cm^2 s^{-1}) [38], $c^b_{O_2}$ is the concentration of oxygen in the bulk (1.2×10^{-6} mol cm^{-3}) [38], and ν is the kinematic viscosity of the solution (0.01 cm^2 s^{-1}) [39].

Figure 4 shows the Koutecky–Levich plots obtained from the RDE data on oxygen reduction at −0.6 V for different carbon nanomaterial-modified electrodes. At this potential, the K–L lines are almost parallel, indicating that the reduction pathway is similar for different carbon materials studied. The intercepts of the extrapolated K–L lines were close to zero, which shows that the process of O_2 reduction is almost entirely under diffusion control. The inset of Fig. 4 compares the n values calculated from the K–L equation at various potentials. For all carbon materials at low overpotentials (E>−0.6 V), the n value was close to two, and the reduction of O_2 produces peroxide which is the final product in this case. At more negative potentials, the value of n gradually increased up to four (the only exception was C824), which indicates that the peroxide formed reduces further in this potential range. The further reduction of peroxide at high overpotentials is in agreement

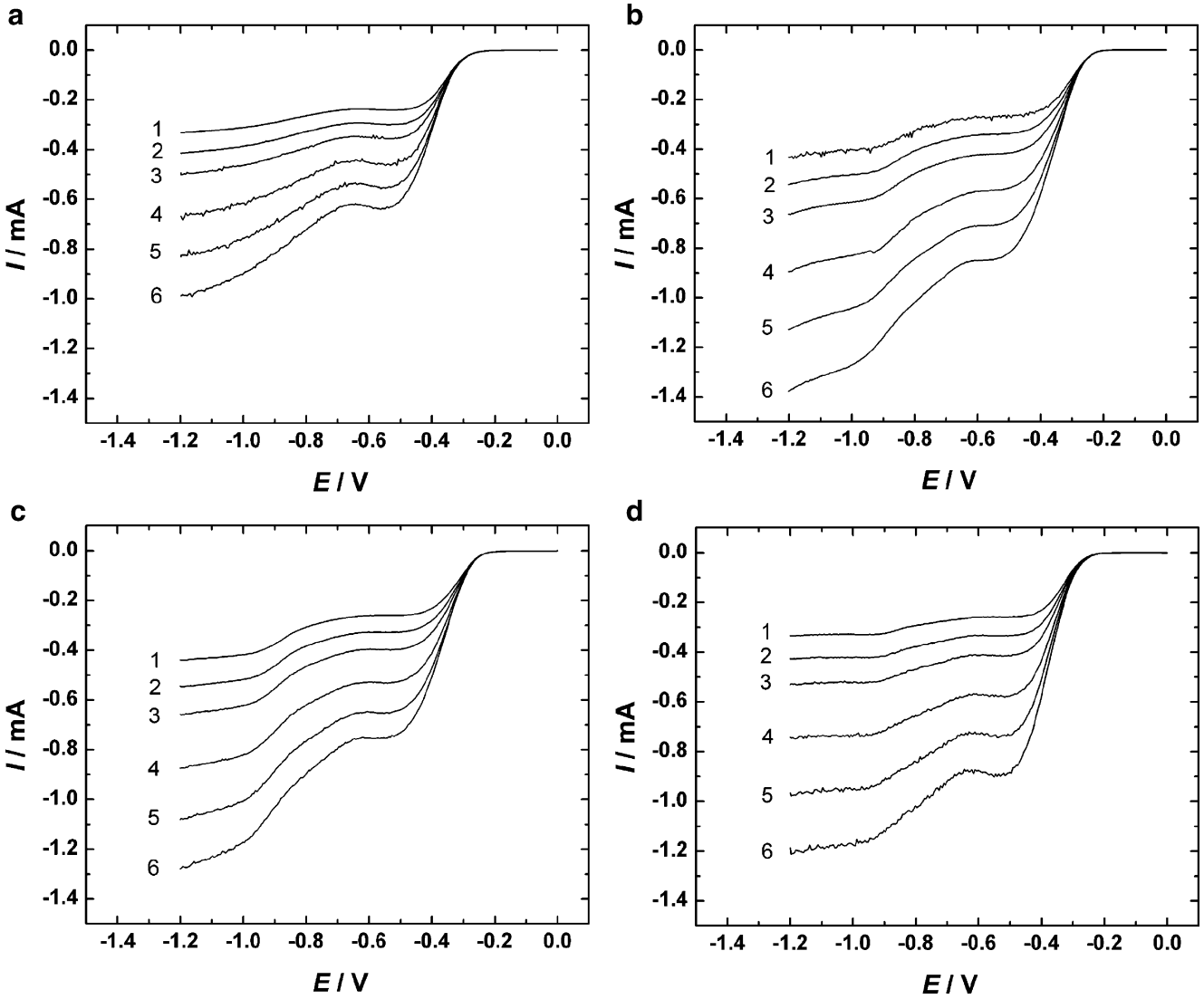

Fig. 3 RDE voltammetry curves for oxygen reduction on carbon nanomaterial-PTFE-modified GC electrodes in O_2-saturated 0.1 M KOH. Nanocarbons used: **a** MWCNT, **b** Vulcan XC72R, **c** C1551, and **d** C824. v=10 mV s^{-1}. ω: *1* 360, *2* 610, *3* 960, *4* 1,900, *5* 3,100, and *6* 4,600 rpm

with previous observations [29]. For most carbon nanomaterials, the n value approaches four, however, there are some subtle differences depending on the carbon materials used.

Rotating ring-disk electrode studies of O_2 reduction

Rotating ring-disk electrode was also used for the investigation of the electrochemical reduction of oxygen on carbon materials deposited on GC. In this case, the nanocarbon–PTFE mixture was annealed at 350 °C for 0.5 h. This is a typical procedure for the preparation of commercial Pt/C catalysts using PTFE as a binder [40]. The PTFE content used (10 wt.%) was found to be suitable for the preparation of catalytically active and stable gas diffusion electrodes [40,41]. The disk currents of oxygen reduction recorded on GC electrodes modified with different carbon nanomaterials are presented in Fig. 5a. The corresponding ring currents are shown in Fig. 5b. At the foot of the polarization curves, the C1551 material shows a higher reduction current than other nanocarbons studied, and this is most probably related to its higher specific surface area (see Table 1). At low overpotentials, the reduction of oxygen yields primarily HO_2^-. This was confirmed by the K–L analysis of the disk current data. The $2e^-$ reduction pathway predominates at E>−0.6 V (see RRDE data analysis below). As can be seen in Fig. 5a, an ill-defined current plateau forms at potentials between −0.6 and −0.4 V for all the nanocarbon-modified electrodes studied. The disk currents at these potentials are close to the diffusion-limiting current for a $2e^-$ reduction of oxygen. In this potential range, the production of peroxide is the

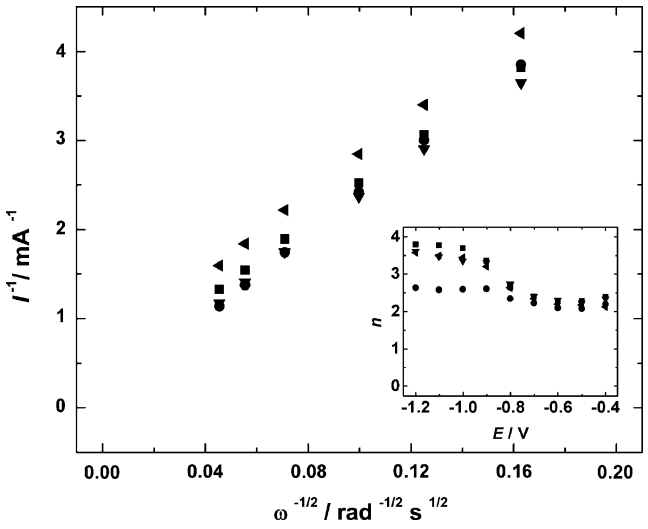

Fig. 4 Koutecky–Levich plots for oxygen reduction on nanocarbon-PTFE-modified GC electrodes at −0.6 V. Nanocarbon materials used: C1551 (■), C824 (●), MWCNT (◀), Vulcan XC72R (▼). *Inset* Potential dependence of n for O_2 reduction on carbon nanomaterial-PTFE-modified GC electrodes in 0.1 M KOH

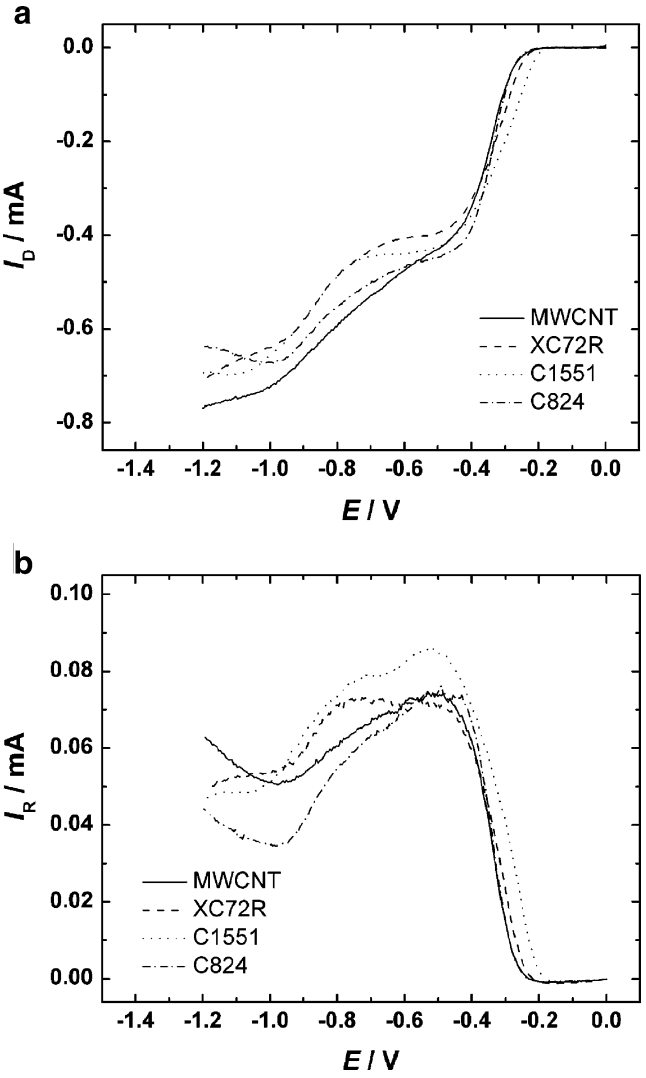

Fig. 5 Ring and disk currents for oxygen reduction on carbon nanomaterial-PTFE-modified GC electrodes in O_2-saturated 0.1 M KOH. v=10 mV s^{-1}. ω=960 rpm. **a** disk and **b** ring currents

highest, which is important from the point of view of the electrosynthesis of hydrogen peroxide [15]. At E<−1 V, the reduction current reaches a limiting value for all the carbon material studied.

The ring currents increase as the rotation rate increases and reach maximum value at *ca*. −0.5 V followed by a decrease of current at more negative potentials. This is a clear indication that the hydrogen peroxide starts to reduce further on the disk electrode, and as a consequence, the contribution of the 4e$^-$ (series) pathway to the overall reduction rate increases. The ring current decrease at E<−0.5 V depends somewhat on the carbon nanomaterial used. For instance, the I_R values for carbon black-PTFE-modified electrode reach a plateau from −0.5 to −0.8 V, indicating that hydrogen peroxide is produced in similar quantities at these potentials. However, for MWCNT-PTFE, C824-PTFE, and C1551-PTFE, there is a tendency for a current decrease in the range of potentials from −0.5 to −1.0 V which reveals that the production of peroxide also decreases.

The RRDE data of O_2 reduction were analyzed using the ratio of disk to ring current [42]. The I_D/I_R vs. $\omega^{-1/2}$ plots were analyzed at E=−0.6 V, and the results for different nanocarbons are shown in Fig. 6. These plots were very similar for all the carbon nanomaterials studied, which means that the I_D/I_R values are almost independent of electrode rotation rate. Similar results were obtained in the work of Appel and Appleby [43]. In all cases, the plots were rather parallel to the x-axis, indicating that the further reduction of peroxide is negligible at this potential. Some scatter in the data could occur because of the nonquantitative detection of the peroxide on the Pt ring. By extrapolating the NI_D/I_R vs $\omega^{-1/2}$ lines to the infinite rotation rate, one can observe intercepts slightly higher than unity. This means that the predominant pathway is the two-electron reduction of oxygen to peroxide which is the final product in this case.

The percentage yield of peroxide formation (Φ) was calculated from [44]

$$\Phi = \frac{200 I_R/N}{I_D + I_R/N} \quad (3)$$

where I_D and I_R are the disk and ring currents, respectively, and N is the collection efficiency. The value of Φ was between 80% and 90% at low overpotentials, and it decreased at potentials more negative than −0.7 V (Fig. 7). At the potentials of the second reduction wave,

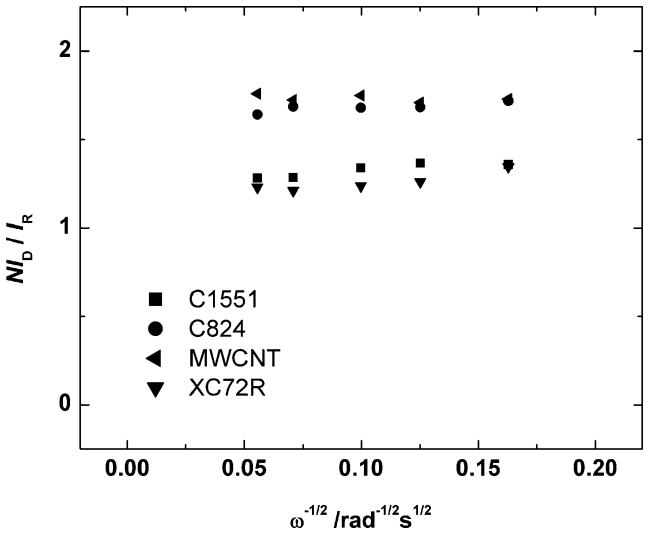

Fig. 6 The dependence of NI_D/I_R on $\omega^{-1/2}$ at −0.6 V for oxygen reduction on carbon nanomaterial-PTFE-modified GC electrodes in 0.1 M KOH

the yield of peroxide was dependent on rotation speed and increased at higher rotation rates. This shows that the number of surface sites at which HO_2^- undergoes electrochemical reduction is limited, and as a consequence, the turnover rate at these sites is insufficient to provide the increased production rate of HO_2^- at high rotation rates, i.e., the reduction of HO_2^- ions becomes less favorable in comparison to the rate of desorption and diffusion in the bulk.

It was shown earlier that the oxidative treatment of high-area carbon materials leads to an increase in the O_2 reduction activity in alkaline solutions [45]. The higher reduction rate could be related to an increase in the number of carbon–oxygen functionalities on their surface. For MWCNTs, it is also well known that some oxygen containing groups are formed during acid treatment. An enhanced electrocatalytic activity for O_2 reduction on anodized GC has been reported [46].

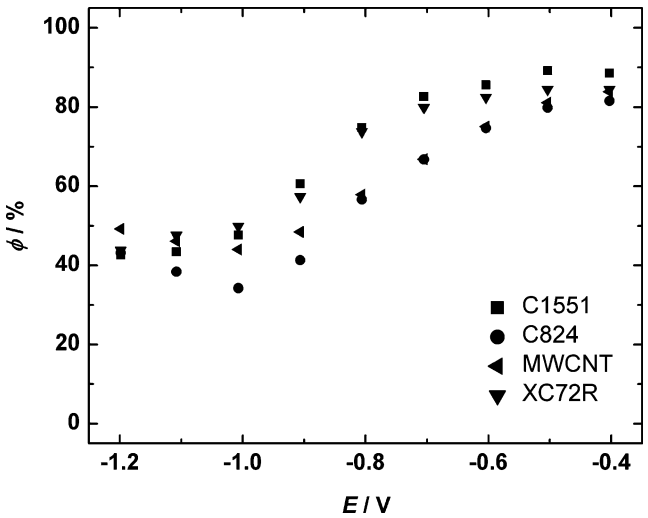

Fig. 7 Dependence of the yield of peroxide formation (Φ) on potential for carbon nanomaterial-PTFE-modified GC electrodes in 0.1 M KOH. Data derived from Fig. 5

Some research groups have proposed that the enhanced O_2 reduction current at prewave potentials in alkaline solutions is caused by quinone-type functionalities on carbon materials [12, 47]. Surface-confined quinones were employed as electrocatalysts for the quantitative reduction of O_2 to hydrogen peroxide [12–14, 46–55]. It is considered that the semiquinone radical anion ($Q^{\bullet-}$) is responsible for the electrocatalysis of oxygen reduction [12–14, 48]. The reduction of oxygen follows an electrochemical–chemical process according to [12]:

$$Q + e^- \rightarrow Q^{\bullet-} \tag{4}$$

$$Q^{\bullet-} + O_2 \xrightarrow{k_c} O_2^{\bullet-} + Q \tag{5}$$

$$O_2^{\bullet-} \xrightarrow{e^-, H_2O} HO_2^- \tag{6}$$

Reaction 5 is considered to be the rate-determining step in the overall reduction of oxygen.

Another important aspect concerning the electrocatalytic properties of carbon nanomaterials is related to their pore size. It appears that micropores are hard to be reached by reacting species [56], and for this reason, the process of O_2 reduction proceeds basically on the surface of carbon particles and in mesopores. Therefore for the nanocarbon-PTFE composites studied, there is only little effect of surface area on the oxygen reduction activity of these materials.

The practical relevance of this work is related to the electrochemical synthesis of hydrogen peroxide in alkaline solutions [15, 57–62]. However, it has been found that peroxide can degrade the surface of carbon materials, and therefore, it is highly challenging to find a carbon-based material, which shows a high electrocatalytic activity for O_2 reduction to peroxide and at the same time possesses an improved corrosion resistance and chemical stability over commercial carbon powders [19, 63]. Up to now, hydrogen peroxide is produced by a chemical route [64]. The electrosynthesis of peroxide has several advantages over the chemical route, and it is particularly attractive to carry out this process using a fuel cell technology [15].

Conclusions

The electrochemical reduction of oxygen has been studied on carbon nanomaterial-modified GC electrodes employing the RDE and RRDE methods. Polytetrafluoroethylene was used as a binder. The results obtained in the present research indicate that these nanocarbon-modified electrodes are highly active for the reduction of oxygen in alkaline solution. It appears that the good electrocatalytic properties of carbon nanomaterials for a $2e^-$ reduction of O_2 at low overpotentials are caused by native quinone-type groups on their surface. Besides surface functionalities, the differences in the structure and porosity of these materials may influence the process of oxygen reduction.

Acknowledgments This research was supported by the Estonian Science Foundation (Grant number 7546). We thank Dr. G. Svensson and Dr. S. Urbonaite, University of Stockholm, for performing TEM measurements of CDC samples. We would also like to thank Mrs. Maike Käärik for carrying out XRD analysis of carbon nanomaterials.

References

1. Tarasevich MR, Sadkowski A, Yeager E (1983) Oxygen electrochemistry. In: Conway BE, Bockris JO'M, Yeager E, Khan SUM, White RE (eds) Comprehensive treatise of electrochemistry, vol 7. Plenum Press, New York, pp 301–398
2. Šljukic B, Banks CE, Compton RG (2005) J Iran Chem Soc 2:1–25
3. Adzic RR (1998) Recent advances in the kinetics of oxygen reduction. In: Lipkowski J, Ross PN (eds) Electrocatalysis. Wiley, New York, pp 197–242
4. Kinoshita K (1992) Electrochemical oxygen technology. Wiley, New York
5. Yeager E (1986) J Mol Catal 38:5–25
6. Yeager E (1984) Electrochim Acta 29:1527–1537
7. Morcos I, Yeager E (1970) Electrochim Acta 15:953–975
8. Taylor RJ, Humffray AA (1975) J Electroanal Chem 64:63–84
9. Xu J, Huang W, McCreery RL (1996) J Electroanal Chem 410:235–242
10. Yang H-H, McCreery RL (2000) J Electrochem Soc 147:3420–3428
11. Yano T, Tryk DA, Hashimoto K, Fujishima A (1998) J Electrochem Soc 145:1870–1876
12. Tammeveski K, Kontturi K, Nichols RJ, Potter RJ, Schiffrin DJ (2001) J Electroanal Chem 515:101–112
13. Sarapuu A, Vaik K, Schiffrin DJ, Tammeveski K (2003) J Electoanal Chem 541:23–29
14. Sarapuu A, Helstein K, Schiffrin DJ, Tammeveski K (2005) Electrochem Solid-State Lett 8:E30–E33
15. Lobyntseva E, Kallio T, Alexeyeva N, Tammeveski K, Kontturi K (2007) Electrochim Acta 52:7262–7269
16. Kostowskyj MA, Gilliam RJ, Kirk DW, Thorpe SJ (2008) Int J Hydrogen Energy 33:5773–5778
17. Qu D (2007) Carbon 45:1296–1301
18. Pirjamali M, Kiros Y (2002) J Power Sources 109:446–451
19. Burchart T (2004) J Power Sources 135:192–197
20. Tryk DA, Cabrera CR, Fujishima A, Spataru N (2005) Oxygen electroreduction on carbon materials. In: Prakash J, Chu D, Scherson D, Enayetullah M, Tae Bae I (eds) Fundamental understanding of electrode processes in memory of Professor Ernest B. Yeager, PV 2003-30. The Electrochemical Society Proceedings, Pennington, New Jersey, pp 45-57
21. Lin YM, Chang YM, Wu PW, Lin P, Li YY, Wu CY, Tsai CF, Yeh KY (2008) J Appl Electrochem 38:507–514
22. Dicks AL (2006) J Power Sources 156:128–141
23. Liu TC, Li YY (2006) Carbon 44:2045–2050
24. Iijima S (1991) Nature 354:56–58
25. Alexeyeva N, Tammeveski K (2007) Electrochem Solid-State Lett 10:F18–F21
26. Shanmugam S, Gedanken A (2006) J Phys Chem, B 110:2037–2044
27. Wang F, Hu S (2006) Electrochim Acta 51:4228–4235
28. Britto PJ, Santhanam KSV, Rubio A, Alonso J, Ajayan PM (1999) Adv Mater 11:154–157
29. Jürmann G, Tammeveski K (2006) J Electroanal Chem 597:119–126
30. Kruusenberg I, Marandi M, Sammelselg V, Tammeveski K (2009) Electrochem Solid-State Lett 12:F31–F34
31. Zhang M, Yan Y, Gong K, Mao L, Guo Z, Chen Y (2004) Langmuir 20:8781–8785
32. Kruusenberg I, Alexeyeva N, Tammeveski K (2009) Carbon 47:651–658
33. Perkson A, Leis J, Arulepp M, Käärik M, Urbonaite S, Svensson G (2003) Carbon 41:1729–1735
34. Tanaka AA, Fierro C, Scherson D, Yeager EB (1987) J Phys Chem 91:3799–3805
35. Alvarez S, Blanco-Lopez MC, Miranda-Ordieres AC, Fuertes AB, Centeno TA (2005) Carbon 43:866–870
36. An KH, Kim WS, Park YS, Choi YC, Lee SM, Chung DC, Bae DJ, Lim SCK, Lee YH (2001) Adv Mater 13:497–500
37. Bard AJ, Faulkner LR (2001) Electrochemical methods, 2nd edn. Wiley, New York
38. Davis RE, Horvath GL, Tobias CW (1967) Electrochim Acta 12:287–297
39. Lide DR (2001) (ed) CRC handbook of chemistry and physics, 82nd edn. CRC Press, Boca Raton
40. Giorgi L, Antolini E, Pozio A, Passalacqua E (1998) Electrochim Acta 43:3675–3680
41. Perez J, Tanaka AA, Gonzalez ER, Ticianelli EA (1994) J Electrochem Soc 141:431–436
42. Wroblowa HS, Pan Y-C, Razumney G (1976) J Electroanal Chem 69:195–201
43. Appel M, Appleby AJ (1978) Electrochim Acta 23:1243–1246
44. Paulus UA, Schmidt TJ, Gasteiger HA, Behm RJ (2001) J Electroanal Chem 495:134–145
45. Horita K, Nishibori Y, Ohshima T (1996) Carbon 34:217–222
46. Vaik K, Schiffrin DJ, Tammeveski K (2004) Electrochem Commun 6:1–5
47. Zhang ZW, Tryk DA, Yeager EB (1984) Effect of surface treatment of glassy carbon on O_2 reduction in alkaline solution. In: Sarangapani S, Akridge JR, Schumm B (eds) Proc. workshop on the electrochemistry of carbon. The Electrochemical Society, Pennington, New Jersey pp 158–178
48. Hossain MS, Tryk D, Yeager E (1989) Electrochim Acta 34:1733–1737
49. Salimi A, Banks CE, Compton RG (2003) Phys Chem Chem Phys 5:3988–3993
50. Mirkhalaf F, Tammeveski K, Schiffrin DJ (2004) Phys Chem Chem Phys 6:1321–1327
51. Vaik K, Sarapuu A, Tammeveski K, Mirkhalaf F, Schiffrin DJ (2004) J Electroanal Chem 564:159–166
52. Vaik K, Mäeorg U, Maschion FC, Maia G, Schiffrin DJ, Tammeveski K (2005) Electrochim Acta 50:5126–5131
53. Maia G, Maschion FC, Tanimoto ST, Vaik K, Mäeorg U, Tammeveski K (2007) J Solid State Electrochem 11:1411–1420

54. Seinberg J-M, Kullapere M, Mäeorg U, Maschion FC, Maia G, Schiffrin DJ, Tammeveski K (2008) J Electroanal Chem 624:151–160
55. Kullapere M, Seinberg J-M, Mäeorg U, Maia G, Schiffrin DJ, Tammeveski K (2009) Electrochim Acta 54:1961–1969
56. Appleby AJ, Marie J (1979) Electrochim Acta 24:195–202
57. Yamada N, Yaguchi T, Otsuka H, Sudoh M (1999) J Electrochem Soc 146:2587–2591
58. Alcaide F, Brillas E, Cabot P-L, Casado J (1998) J Electrochem Soc 145:3444–3449
59. Brillas E, Alcaide F, Cabot P-L (2002) Electrochim Acta 48:331–340
60. Alcaide F, Brillas E, Cabot P-L (2004) J Electroanal Chem 566:235–240
61. Alcaide F, Brillas E, Cabot P-L (2002) J Electrochem Soc 149: E64–E70
62. Gonzalez-Garcia J, Banks CE, Šljukić B, Compton RG (2007) Ultrason Sonochem 14:405–412
63. Franco AA, Gerard M (2008) J Electrochem Soc 155:B367–B384
64. Campos-Martin JS, Blanco-Brieva G, Fierro JLG (2006) Angew Chem Int Ed 45:6962–6984